JGR Oceans

RESEARCH ARTICLE

10.1029/2025JC022899

# ENSO Influences Subsurface Marine Heatwave Occurrence in the Kuroshio Extension

**Mitchell Chandler (he/him)[1,2], Janet Sprintall[1], and Nathalie V. Zilberman[1]**

[1]Scripps Institution of Oceanography, University of California San Diego, La Jolla, CA, USA, [2]The Wilderness Society, Washington, DC, USA

**Key Points:**

- Subsurface MHWs along an HR-XBT transect east of Japan are examined using a new multidecadal temperature time series with 10-day resolution
- A significant increase in surface and subsurface Kuroshio MHW days per year is driven by a significant warming trend in the Kuroshio
- Subsurface MHWs are more common during El Niño where the stronger Kuroshio Extension and its southern recirculation gyre intersect the transect

**Supporting Information:**

Supporting Information may be found in the online version of this article.

**Correspondence to:**

M. Chandler,
mitchell.chandler.po@gmail.com

**Citation:**

Chandler, M., Sprintall, J., & Zilberman, N. V. (2025). ENSO influences subsurface marine heatwave occurrence in the Kuroshio extension. *Journal of Geophysical Research: Oceans*, *130*, e2025JC022899. https://doi.org/10.1029/2025JC022899

Received 19 MAY 2025
Accepted 20 AUG 2025

**Author Contributions:**

**Conceptualization:** Mitchell Chandler, Janet Sprintall, Nathalie V. Zilberman
**Data curation:** Mitchell Chandler, Janet Sprintall
**Formal analysis:** Mitchell Chandler
**Funding acquisition:** Janet Sprintall, Nathalie V. Zilberman
**Investigation:** Mitchell Chandler
**Methodology:** Mitchell Chandler
**Project administration:** Mitchell Chandler
**Resources:** Janet Sprintall, Nathalie V. Zilberman
**Software:** Mitchell Chandler
**Supervision:** Janet Sprintall, Nathalie V. Zilberman
**Validation:** Mitchell Chandler



**Abstract** Extreme ocean temperature events, also known as marine heatwaves (MHWs), can have devastating consequences for ecosystems, communities, and economies. However, the ability to understand and predict MHWs beneath the sea surface is limited by a scarcity of subsurface observations. Here, we combined in situ temperature observations from a High-Resolution eXpendable BathyThermograph (HR-XBT) transect in the northwest Pacific Ocean with satellite observations to produce a multidecadal (1993–2022) subsurface temperature time series with 10-day temporal resolution. This novel time series was used to examine MHWs between the surface and 800-m deep in the Kuroshio-Kuroshio Extension region east of Japan. The length of this 30-year time series also permitted exploration of long-term trends and interannual variability in subsurface temperature. Variability in the Kuroshio-Kuroshio Extension system is found to exert a strong control on the occurrence of MHWs along the transect. Throughout the upper 800-m of the water column, Kuroshio warming drove a significant increase in Kuroshio MHW days per year. Notably, the largest mean MHW event intensities were observed in the subsurface at every location along the transect rather than at the sea surface. Strengthening of the Kuroshio Extension and its southern recirculation gyre during El Niño drove a significant increase in subsurface MHWs where the intensified current system intersected the transect. In contrast, surface MHW occurrence along the transect was not influenced by the El Niño-Southern Oscillation (ENSO). Clearly, relying only on sea surface temperature observations does not provide the full picture of MHWs in this highly dynamic region.

**Plain Language Summary** Marine heatwaves (MHWs)—the ocean equivalent to the atmospheric heatwaves we experience on land—are periods of unusually warm water. These events have the potential to cause devastating economic impacts. Although MHWs occur throughout the ocean, most studies have focused only on events at the sea surface due to the availability of long-term satellite measurements. Fewer long-term time series exist beneath the sea surface. Here, we combined long-term satellite measurements of the surface with repeated subsurface temperature measurements collected along a shipping route in the northwest Pacific Ocean to produce a new temperature time series between the surface and 800-m deep. This multidecadal time series was used to examine subsurface MHWs in the Kuroshio and Kuroshio Extension—strong ocean currents east of Japan. We found that, since 1993, warming temperatures in the Kuroshio have caused an increase in the number of subsurface MHW days per year. In addition, subsurface MHWs occurred more often during El Niño conditions due to a strengthening of the Kuroshio Extension. This information could aid in designing and implementing MHW adaptation plans in this region.

## 1. Introduction

Marine heatwaves (MHWs) are prolonged periods of anomalously warm water (Hobday et al., 2016). These events can have devastating consequences for marine ecosystems (Cavole et al., 2016; Mills et al., 2013; Smale et al., 2019; Smith et al., 2021, 2023). Such extreme ocean temperatures can also impact regional weather by influencing surface air temperature, humidity, winds, and/or precipitation (Pathmeswaran et al., 2022; Sugimoto et al., 2021; Tochimoto & Iizuka, 2022). The potential economic impacts of MHWs can thus reach into the billions of dollars (Smith et al., 2021).

Due to the extensive spatial and temporal coverage provided by sea surface temperature (SST) observations, most MHW studies have focused only on events at the sea surface. Yet SST variability is often not representative of subsurface temperature variability. Differences between surface and subsurface temperature arise, in part, because of the different forcing mechanisms driving temperature variability, and consequently MHWs, at the

**Visualization:** Mitchell Chandler
**Writing – original draft:** Mitchell Chandler
**Writing – review & editing:** Mitchell Chandler, Janet Sprintall, Nathalie V. Zilberman

surface and in the subsurface (e.g., Elzahaby et al., 2021; Großelindemann et al., 2022; Xu et al., 2024). As such, subsurface MHWs can occur independently of anomalous warming at the sea surface and can have greater intensities than surface MHWs (Hu et al., 2021; Schaeffer et al., 2023; Schaeffer & Roughan, 2017). Subsurface intensification is also thought to be a common feature of surface MHWs in western boundary current (WBC) regions (Elzahaby & Schaeffer, 2019; Welch et al., 2025; Zhang et al., 2023). Ecosystem impacts of these MHWs are therefore often amplified at depth, where many commercially important species are found (e.g., Cai et al., 2020; Mills et al., 2013). The ability to observe, understand, and predict MHW events below the sea surface is thus a priority for the MHW community (Oliver et al., 2021).

In this study, we focus on MHWs in the Kuroshio, the WBC of the North Pacific Ocean. The Kuroshio holds cultural, economic, and climatic importance for nearby countries (Ando et al., 2021) as it is an important spawning and nursery area for fish (Fujioka et al., 2018; Kitagawa et al., 2010; Yatsu, 2019) and exerts an important influence on regional weather and climate (Bond & Cronin, 2008; Nonaka & Xie, 2003; Qiu et al., 2014; Sasaki et al., 2012; Sugimoto et al., 2021). Over recent decades, warming has been observed at the surface along the path of the Kuroshio (Wang et al., 2016) and in the subsurface at 137°E (Oka et al., 2017). This warming has occurred despite a decreasing trend in Kuroshio mass transport (Chandler et al., 2022a; Liu et al., 2021; Wang et al., 2016), with surface warming instead being driven by warming of source waters (Wang et al., 2016). Surface warming is projected to drive an increase, relative to a fixed baseline, in surface MHW occurrence within the Kuroshio and Kuroshio Extension over the course of the century (Kawakami et al., 2024). However, comparable trends in subsurface MHWs are yet to be demonstrated. The El Niño-Southern Oscillation (ENSO) has also been shown to influence MHW occurrence in the North Pacific Ocean (e.g., Gregory et al., 2024). Although recent studies indicate essentially no relationship between ENSO and surface MHW occurrence in the Kuroshio-Kuroshio Extension region (Gregory et al., 2024; Holbrook et al., 2019; Sen Gupta et al., 2020), it is unknown whether this same lack of relationship extends into the subsurface.

Multidecadal and high-resolution measurements are essential for observing, understanding, and predicting MHWs. Yet such time series are rare in the ocean's subsurface. The High-Resolution eXpendable BathyThermograph (HR-XBT) network provides measurements of ocean temperature between the surface and more than 800-m deep along fixed transects, with some transects having been occupied for more than 30 years (Goni et al., 2019). These subsurface temperature observations are at high spatial resolutions ($O$(1–10)-km), but lower temporal resolutions (nominally four occupations per year). However, HR-XBT and sea level anomaly (SLA) observations have a close relationship that can be exploited to enhance the temporal resolution of these subsurface temperature time series (Chandler et al., 2022a; Gilson et al., 1998; Ridgway et al., 2008; White & Tai, 1995; Willis et al., 2003).

Here, we examine the occurrence of subsurface MHWs along an HR-XBT transect intersecting the Kuroshio and Kuroshio Extension using a novel 30-year synthetic temperature time series. This new time series is produced from complementary HR-XBT and satellite observations (Section 2.2). Along the transect, warming trends in the Kuroshio (Section 3.1) have led to an increase in surface and subsurface MHW days per year within the Kuroshio (Section 3.2). The largest mean MHW event intensities and durations along the transect occur at depth (Section 3.3). Subsurface MHWs are more common during El Niño where an intensified Kuroshio Extension intersects the transect (Section 3.4). In contrast, surface MHW occurrence along the transect is not influenced by ENSO (Section 3.4). We conclude in Section 4 with a summary and implications of this work.

## 2. Data and Methodology

### 2.1. Data

Subsurface temperature observations were obtained from measurements along HR-XBT transect PX40 (Figure 1), which runs between Yokohama, Japan and Honolulu, Hawai'i. This transect crosses the Kuroshio at approximately 34.5°N, just south of where the Kuroshio separates from the coast to form the Kuroshio Extension. To focus on the WBC system, only observations west of 150°E were used. HR-XBT temperature measurements were objectively mapped onto a 10-m depth grid between the surface and 800-m deep and a 0.1° along-transect longitudinal grid (Roemmich, 1983). At the time of this study, PX40 had been occupied 41 times since 2012.

The 2015–2022 temperature climatology from the 1/4° World Ocean Atlas 2023 (Locarnini et al., 2024) was used to adjust PX40 observations onto the mean transect. This climatology covers a similar time period as the PX40

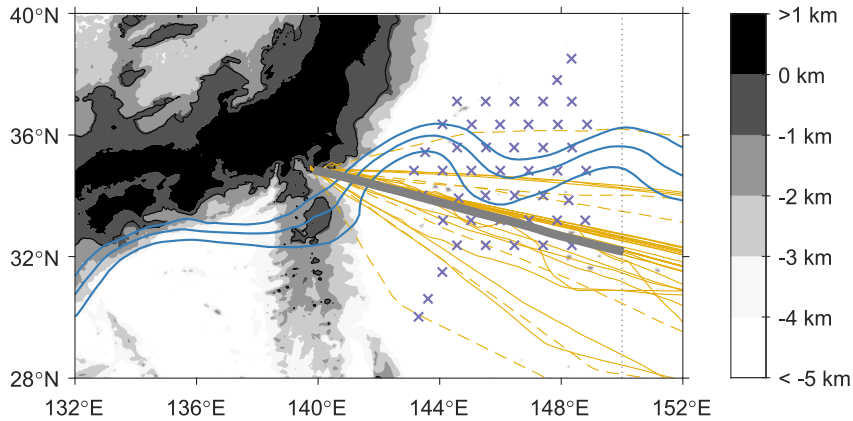


**Figure 1.** PX40 mean transect (thick gray line) overlain on the bathymetry of the northwest Pacific Ocean. The black contour line is the 800-m isobath. Gold lines show the paths of all individual PX40 transects (dashed transects were not used in this study due to being either too far from the mean transect or more recent than available satellite altimetry observations). Purple crosses locate the PIES/CPIES deployed during the Kuroshio Extension System Study (2004–2006). Blue lines are the 0.9-m, 1.1-m, and 1.3-m absolute dynamic topography contours averaged over 1993–2022 and represent the mean path of the Kuroshio and Kuroshio Extension. The thin dotted line is at 150°E.

observations. World Ocean Atlas 2023 has up to 102 standard depth levels of varying resolution and was therefore linearly interpolated onto the same 10-m depth grid as the HR-XBT temperature data.

Daily SLA was from the 1/4° "Global ocean gridded L4 sea surface heights and derived variables reprocessed" product (CMEMS, 2024a). Daily SST was from the 1/4° "NOAA daily optimum interpolation sea surface temperature version 2.1" product (Huang et al., 2021). This SST product is independent of HR-XBT observations (Huang et al., 2021; Willis et al., 2003). Both the SLA and SST time series spanned the period 1 January 1993–30 April 2023.

The maximum climatological surface mixed layer depth along PX40 was obtained from the 1° "Mixed layer depth climatology computed with a density threshold criterion of 0.03 kg $m^{-3}$ from 10-m depth value" product (de Boyer Montégut et al., 2004).

The Oceanic Niño Index (ONI) was used to identify El Niño (ONI > +0.5°C) and La Niña (ONI < −0.5 °C) periods between 1993 and 2022. ONI is computed based on the 3-month running mean of SST anomalies in the Niño 3.4 region and, here, was taken to represent the central month of each 3-month average. These same processing steps were applied to the Niño 3 index used to identify eastern Pacific El Niño conditions and the Niño 4 index used to identify central Pacific El Niño conditions (e.g., Capotondi et al., 2015; Wang et al., 2024).

Monthly zonal and meridional velocities from the 1/12° Global Ocean Physics Reanalysis 12V1 (GLORYS; Lellouche et al., 2021) were used to provide spatial context for the state of the Kuroshio Extension system between 1993 and 2020. GLORYS was validated against monthly PX40 cross-transect velocities between 2004 and 2019 from Chandler et al. (2022a). The two velocity products agreed well, although the core of the Kuroshio was shifted slightly offshore at depth in GLORYS (Text S1 in Supporting Information S1; Figure 2).

### 2.2. Synthetic Temperature Time Series Development

All 41 individual occupations of PX40 were averaged to obtain a first guess of the mean location of the PX40 transect. Individual transects that reached a maximum latitudinal distance of more than 4° from the mean transect were removed, and the mean was recalculated until all remaining transects were within 4° of latitude. Three occupations were removed through this procedure. A further three occupations after April 2023 were also removed as, at the time of analysis, SLA data were not yet available. This study therefore utilized 35 occupations of PX40 between November 2012 and March 2023 (Figure 1). Every month of the year had at least one occupation. Each ENSO phase (El Niño, La Niña, and neutral) had at least eight occupations.

Individual transects do not exactly follow the mean PX40 transect (Figure 1). Therefore, for each occupation, the difference in climatological temperature between the occupied transect and the mean transect was used to correct

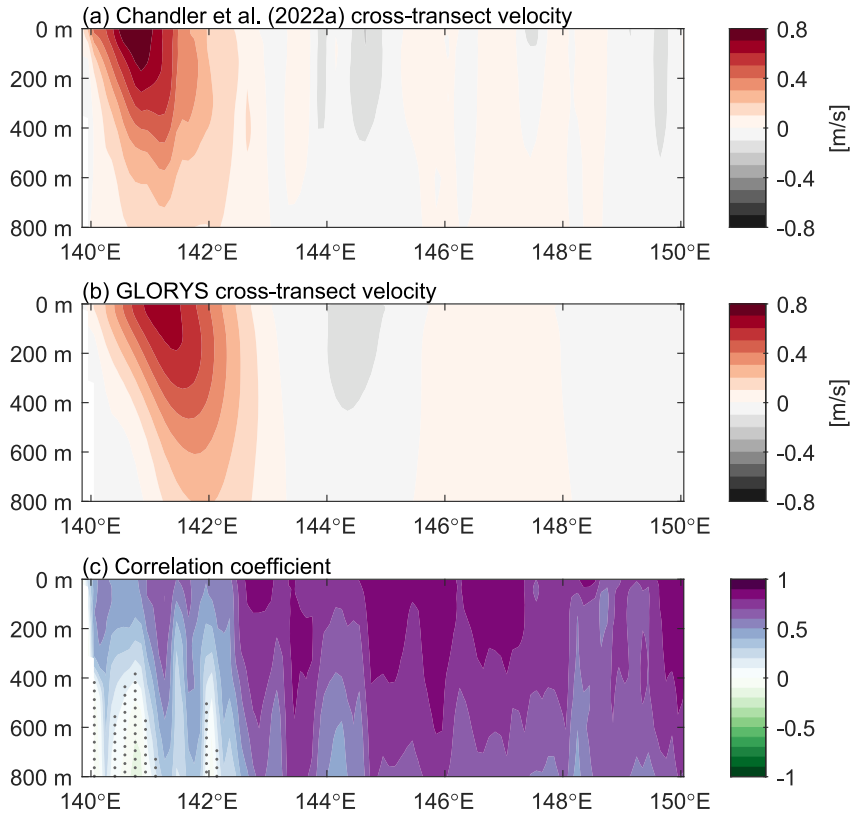


**Figure 2.** Time mean of the 2004–2019 monthly cross-transect velocity time series from (a) Chandler et al. (2022a) and (b) GLORYS. A positive velocity is northward. (c) Correlation coefficients between the Chandler et al. (2022a) and GLORYS velocity anomalies. Stippling identifies where correlations are not significant at the 95% significance level (effective degrees of freedom computed following Von Storch and Zwiers (1999)).

for variability in ship tracks. Deviations of individual transects from the mean transect were typically small. As such, surface biases (i.e., the climatological difference in surface temperature between the mean transect and each individual occupation minus the difference between the mean transect and each individual occupation from 10-day averaged SST) also tended to be small. Over the transect, the mean surface bias was 0.01°C, median surface bias was negligible (<|0.01|°C), and root mean square surface bias was 0.25°C. Nevertheless, highly localized features could introduce errors. For example, an occupation measuring a MHW would project the anomalously high temperatures onto the mean transect even if the MHW was of small meridional extent and did not occur at the mean transect.

Daily SLA and SST were interpolated onto the mean transect and averaged over the 10 days following the start date of each PX40 occupation. A 10-day temporal resolution is consistent with the cycle duration of the satellite altimetry reference missions. The 35-transect seasonal cycle, computed via least squares fitting an annual harmonic, semiannual harmonic, and mean, was removed to obtain temporal anomalies ($T'(z)_{px40}$, $SLA'_{px40}$, and $SST'_{px40}$) that were all referenced to the same time period (November 2012–March 2023, i.e. the PX40 time period). Comparison of these PX40-period SLA and SST seasonal cycles against those computed using the full (January 1993–April 2023) time series confirmed that the temporal coverage of the 35 PX40 occupations was able to resolve the seasonal cycle.

There was a strong relationship between $SLA'_{px40}$ and $T'(z)_{px40}$ below the surface mixed layer, while $SST'_{px40}$ was better correlated with surface and near-surface temperature anomalies (not shown, see also Willis et al., 2003). Therefore, to take advantage of their individual strengths, the 10-day averaged $SLA'_{px40}$ and $SST'_{px40}$ were fit to observed $T'(z)_{px40}$ at the times of the 35 PX40 occupations using a multiple linear regression (e.g., Ridgway et al., 2008; Willis et al., 2003) as follows:

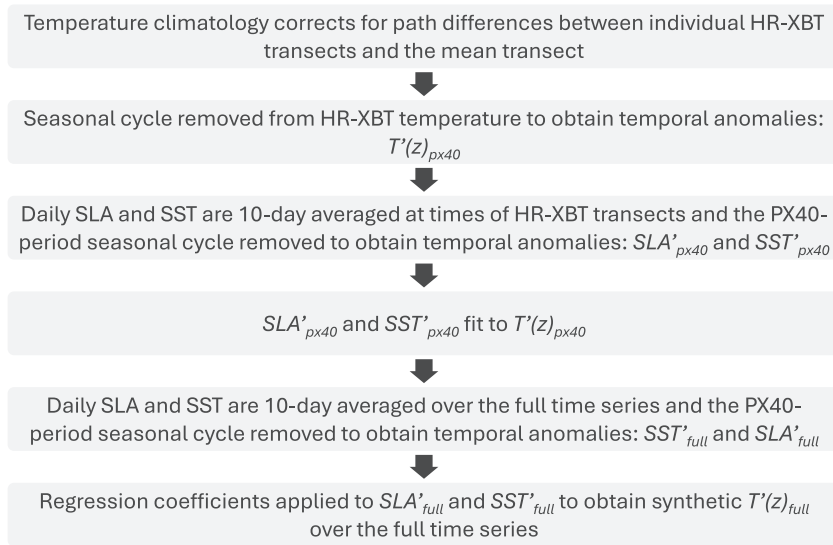


**Figure 3.** Diagram summarizing the key steps in developing the synthetic subsurface temperature anomaly time series. Terminology is as follows: HR-XBT, High-Resolution eXpendable BathyThermograph; $T'(z)$, temperature anomaly as a function of depth; SLA, Sea Level Anomaly; and SST, Sea Surface Temperature.

$$T'(x,z,t) \approx \alpha(x,z) \cdot SLA'(x,t) + \beta(x,z) \cdot SST'(x,t) \quad (1)$$

where $x$ is location along the transect, $z$ is depth, $t$ is time, and $\alpha$ and $\beta$ are regression coefficients.

The full (January 1993–April 2023) SLA and SST time series were then averaged every 10 days, and the PX40-period seasonal cycles removed. The regression coefficients ($\alpha$ and $\beta$) were applied (Equation 1) to these 10-day averaged $SLA'_{full}$ and $SST'_{full}$ time series to obtain estimates of 10-day averaged synthetic $T'(z)_{full}$ from 0-m down to 800-m deep over the full January 1993–April 2023 time period. The above procedure is summarized in Figure 3. Note that usage of the full subscript will be dropped from the text hereafter.

### 2.3. Synthetic Temperature Time Series Validation

The method (Figure 3) was validated using a leave-one-out approach where regression coefficients ($\alpha$ and $\beta$; Equation 1) were recalculated using all PX40 occupations bar one, and a synthetic estimate was computed for the withheld occupation (e.g., Gilson et al., 1998). This procedure was repeated 35 times, such that all PX40 occupations were withheld once. The resulting 35 synthetic estimates compared favorably with the 35 HR-XBT observations, albeit with reduced variability and with small discrepancies in the surface mixed layer (Figure 4). Standard deviations demonstrated a similar structure (Figures 4a and 4b) but with smaller values for the synthetic estimates than the observations. Correlations between synthetic and observed $T'(z)_{px40}$ were significant ($p<0.05$) almost everywhere, except for some near-surface regions and at the very western edge (Figure 4c). Likewise, the root mean square signal of observed $T'(z)_{px40}$ was greater than the root mean square error (RMSE) between synthetic and observed $T'(z)_{px40}$ except for a few regions near the surface and at the western edge (Figure 4d). Averaged over the entire section, RMSE between synthetic and observed $T'(z)_{px40}$ was 1.12°C.

To validate the ability of the method to be extended back in time through use of the satellite record prior to PX40 observations (i.e., January 1993–October 2012), synthetic $T'(z)$ was compared against independent observations from the Kuroshio Extension System Study (KESS). During KESS, an array of 46 Pressure recording Inverted Echo Sounders/Current and Pressure recording Inverted Echo Sounders (PIES/CPIES) were deployed in the Kuroshio Extension east of Japan (Figure 1) for 16 months between 2004 and 2006 (Donohue et al., 2010). Here, the objectively mapped subsurface temperature fields from the KESS array (Donohue et al., 2010) were interpolated onto the same PX40 transect and 10-m depth grid as synthetic $T'(z)$, averaged into 10-day periods, and

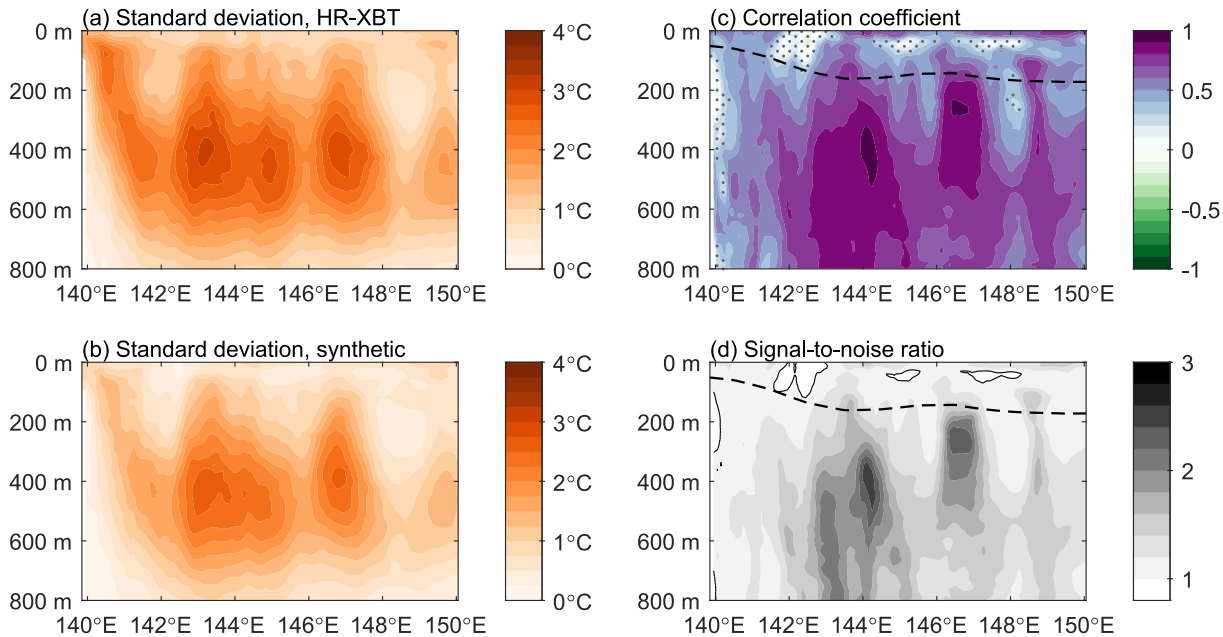


**Figure 4.** Standard deviations of (a) HR-XBT observed temperature anomalies and (b) synthetic temperature anomalies at the times of PX40 occupations. (c) Correlation coefficients between HR-XBT observed and synthetic temperature anomalies. Stippling is where correlations are not significant at the 95% significance level (each occupation considered independent). (d) Ratio of the root mean square signal of HR-XBT observed temperature anomalies to the root mean square error between HR-XBT observed and synthetic temperature anomalies. The black contour identifies a ratio of 1. The black dashed line in (c) and (d) is the maximum climatological mixed layer depth.

deseasoned by subtracting the PX40-period seasonal cycle. KESS and synthetic $T'(z)$ were compared over the longitude range that provided the longest time period (June 2004–September 2005) of consistently good quality KESS data, and were found to compare favorably (Figure 5). The RMSE between KESS and synthetic $T'(z)$ averaged over the entire section was 1.16°C, similar to the 1.12°C from the leave-one-out validation above, which provided confidence that satellite observations could indeed be used to extend the synthetic $T'(z)$ time series back in time prior to PX40 observations. However, there is no guarantee the same regression coefficients will continue to hold into the future given expected climate shifts and resulting nonstationarity (e.g., Litzow et al., 2020).

### 2.4. Marine Heatwave Identification

The synthetic $T'(z)$ time series (rereferenced to the 1993–2022 time mean) was used to examine extreme ocean temperature events (i.e., MHWs) between the surface and 800-m deep over the 1993–2022 time period.

Qualitatively, a MHW is defined as a prolonged period of anomalously warm water at a particular location (Hobday et al., 2016). One commonly used quantitative definition is where daily ocean temperatures are warmer than the 90th percentile climatology for a period of five or more days, with events separated by two or less days considered as a single event (Hobday et al., 2016). However, the qualitative definition offers flexibility, including in the temporal resolution of the time series (Farchadi et al., 2025; Hobday et al., 2016; Oliver et al., 2021). For example, numerous studies have used monthly resolution temperature time series where MHWs were thus defined as extreme events lasting at least 1 month (e.g., Jacox et al., 2020; Jacox et al., 2022; Scannell et al., 2016; Gregory et al., 2024; von Kietzell et al., 2022; Zhou et al., 2024).

Here, MHWs were defined as when synthetic $T'(z)$ was above the 90th percentile temperature anomaly threshold. This threshold varied with $x$ and $z$ but, because the seasonal cycle had already been removed from the synthetic $T'(z)$ time series, was constant in time. Due to the 10-day resolution of the time series, each instance where $T'(z)$ exceeded the 90th percentile threshold was defined as a MHW. MHW conditions therefore occurred during 10% of the study time period. MHW conditions occurring in consecutive 10-day periods were considered a single MHW event.

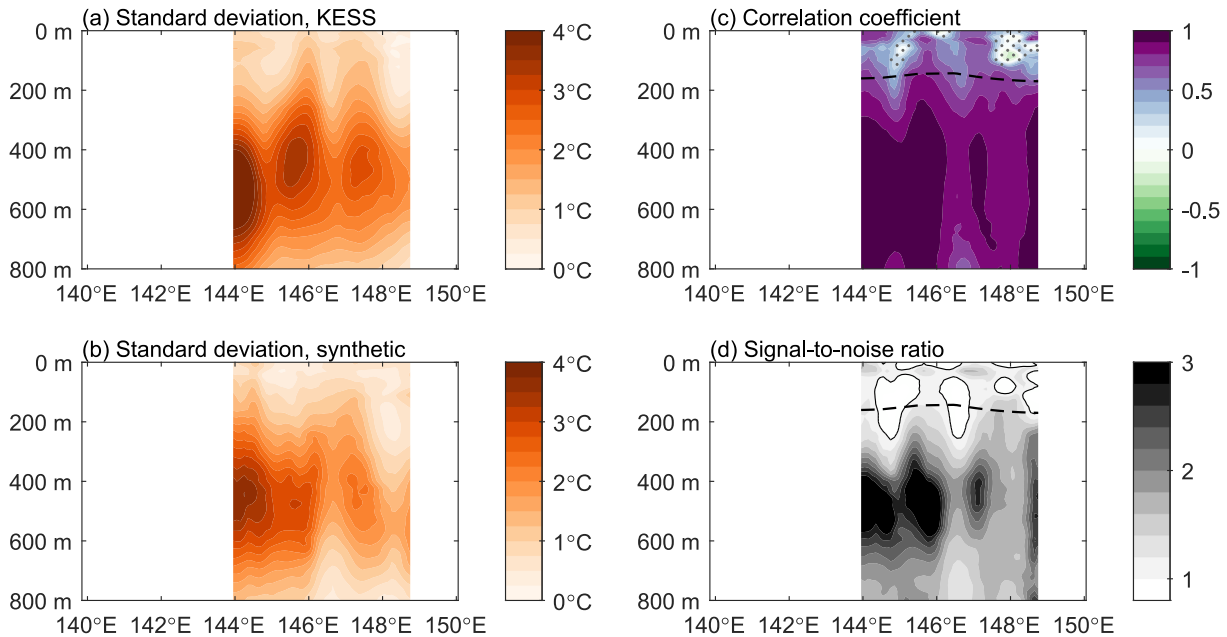


**Figure 5.** Standard deviations of (a) Kuroshio Extension System Study (KESS) temperature anomalies and (b) synthetic temperature anomalies between June 2004 and September 2005. (c) Correlation coefficients between KESS and synthetic temperature anomalies. Stippling is where correlations are not significant at the 95% significance level (effective degrees of freedom computed following Von Storch and Zwiers (1999)). (d) Ratio of the root mean square signal of KESS temperature anomalies to the root mean square error between KESS and synthetic temperature anomalies. The black contour identifies a ratio of 1. The black dashed line in (c) and (d) is the maximum climatological mixed layer depth.

Following Hobday et al. (2016), MHW intensity was defined as $T'(z)$, that is, the temperature anomaly relative to the 1993–2022 time mean. Only mean event intensity was considered here as the reduced variability in the synthetic temperature time series compared to observations (Figures 4 and 5) meant that maximum event intensity was likely underestimated. Higher temporal resolution observations (e.g., daily) have more variability, and typically larger maximum values, than those based on longer (e.g., 10-day or monthly) time means (Hobday et al., 2016).

To examine whether there had been a change in MHW occurrence over the 30-year time series, linear trends were fit at every grid point $(x, z)$ to the number of MHW days per year. Trend significance was assessed using a two-tailed $t$ test (Draper & Smith, 1998) where each year was considered independent. Linear trends were also computed for the synthetic $T'(z)$ time series with significance assessed using a two-tailed $t$ test where the effective degrees of freedom was calculated using the integral time scale (Emery & Thomson, 2001). Temperature trends were found to impact MHW identification along PX40 (see Section 3.2), and so MHWs were also identified using the detrended synthetic $T'(z)$ time series so that the influence of factors other than long-term ocean warming could be examined.

To examine the influence of one such factor, ENSO, on MHW occurrence along the transect, the percentage of time when MHW conditions were experienced during El Niño and La Niña was examined. A chi-square test was used to determine if MHW occurrence was significantly different from the expected 10% occurrence rate during each ENSO phase. The detrended synthetic $T'(z)$ time series was used to examine MHW occurrence in the subsurface (i.e., below the maximum climatological surface mixed layer depth), and the detrended 10-day averaged $SST'$ time series was used to examine MHW occurrence at the surface. However, because synthetic $T'(z)$ demonstrated limited ability in reproducing near-surface temperature anomalies (Figures 4 and 5), MHW occurrence during each ENSO phase was not examined within the surface mixed layer. Other climate modes (namely the Pacific Decadal Oscillation (PDO), Indian Ocean Dipole (IOD), and Pacific-Japan pattern) were also considered, but, compared with ENSO, demonstrated a weaker relationship with synthetic $T'(z)$ (Text S2 in Supporting Information S1). ENSO also demonstrated a stronger causal relationship with synthetic $T'(z)$.

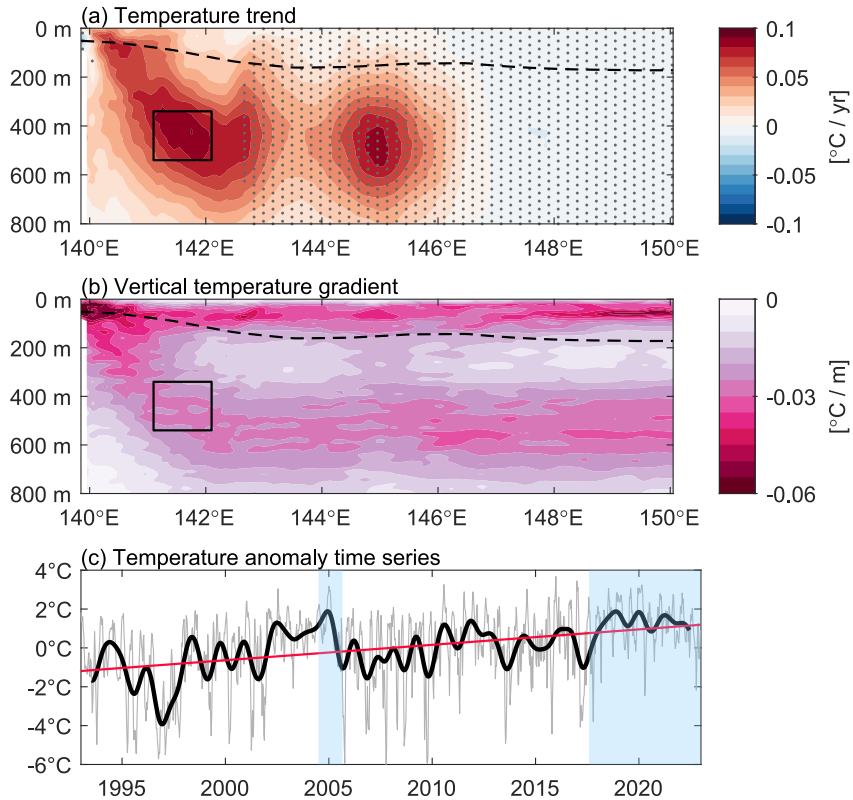


**Figure 6.** (a) Temperature trends over 1993–2022. Stippling is where trends are not significant at the 95% significance level. (b) Vertical temperature gradients in the 1993–2022 time mean temperature. The black dashed line in (a) and (b) is the maximum climatological mixed layer depth, and the black box indicates the region plotted in (c). (c) Temperature anomaly time series over 1993–2022, area-averaged in the region where Kuroshio warming trends were largest. The thin gray line is the raw (10-day) time series, the thick black line is the annually low-pass filtered time series, and the red line is the trend. Light blue shading identifies times of the Kuroshio large meander.

Relative information flow rates (Liang, 2014, 2015) from each climate mode to the annually low-pass filtered first principal component of detrended synthetic $T'(z)$ were 34% for ENSO, 23% for IOD, and 16% for PDO.

## 3. Results and Discussion

### 3.1. Temperature Trends

The 30-year length of the synthetic temperature time series allowed multidecadal subsurface temperature trends to be estimated with a high degree of confidence (Figures 6a and 6c). Over 1993–2022, there was a significant warming trend at transect PX40 between 139.9°E and 142.9°E that extended throughout the upper 800-m, reaching 0.09°C $yr^{-1}$ within the subsurface (Figure 6a). The location of this significant warming coincides with the mean location of the Kuroshio jet (Figure 2). Kuroshio warming at the surface was typically reduced compared to the subsurface, although still significant, with a mean warming trend of 0.02°C $yr^{-1}$. The observed surface and subsurface warming trends along PX40 became nonsignificant offshore of the Kuroshio and then switched to a nonsignificant cooling trend east of approximately 146.8°E (Figure 6a).

The surface warming rate in the Kuroshio at PX40 (Figure 6a) is consistent with SST warming trends in the upstream Kuroshio over 1993–2013 (Wang et al., 2016), and with projected SST warming trends over the course of this century in the Kuroshio-Kuroshio Extension region from a high-resolution (1/11° longitude × 1/10° latitude) ocean model (Kawakami et al., 2024). However, there are very few long time series of subsurface temperature available in the Kuroshio. One of these is the 137°E repeat hydrographic transect that intersects the Kuroshio south of Japan, upstream of PX40, and which has been occupied annually since 1967 and then semi-annually since 1972 (Oka et al., 2018). Using wintertime observations over the period 1967–2016, Oka et al. (2017) found a warming trend in the Kuroshio at 137°E that, much like our result at PX40 (Figure 6a), was

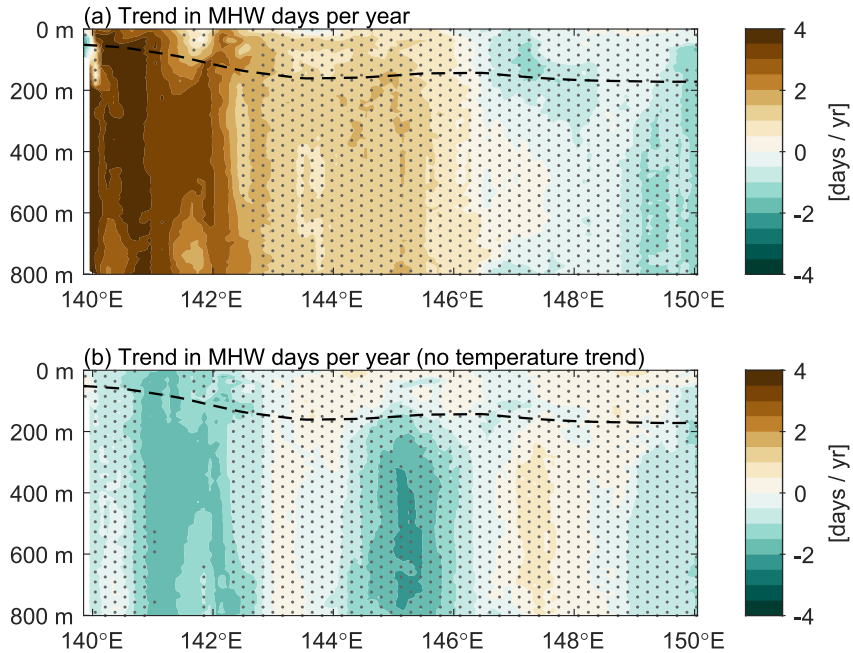


**Figure 7.** Trends over 1993–2022 in (a) marine heatwave (MHW) days per year and (b) MHW days per year when the 1993–2022 temperature trend is removed. Stippling is where trends are not significant at the 95% significance level. The black dashed line is the maximum climatological mixed layer depth.

largest in the subsurface between roughly 200 and 600-dbar. However, Kuroshio warming trends at 137°E between 1967 and 2016 were roughly half those observed at PX40 between 1993 and 2022. The larger subsurface temperature trends in our more contemporary data set therefore suggest an acceleration of subsurface warming within the Kuroshio.

Oka et al. (2017) attributed Kuroshio subsurface warming at 137°E to a decrease in Kuroshio large meander occurrence. However, large meander events (Yoshida et al., 2006) have minimal impact on the path of the Kuroshio at PX40 (e.g., Chandler et al., 2022a; Kawabe, 1985, 1995). Additionally, the Kuroshio has been in an ongoing large meander state since August 2017 (Qiu et al., 2023; Yoshida et al., 2006), coinciding with some of the warmest subsurface temperature anomalies at PX40 (Figure 6c). Therefore, decreasing large meander occurrence cannot explain the significant subsurface warming trend between 1993 and 2022 at PX40. Strengthening of advective heat transport within the Kuroshio also seems an unlikely driver of subsurface warming given that Kuroshio mass transport has decreased over 2004–2019 at PX40 (Chandler et al., 2022a) and over 1998–2013 further upstream at Tokara Strait (Liu et al., 2021). This decrease in mass transport has been driven by vertical pycnocline displacement (i.e., heave) caused by wind stress curl changes over the North Pacific Ocean (Liu et al., 2021). Heaving of isotherms, which produces large temperature changes where vertical temperature gradients are steep, could be driving subsurface warming in the Kuroshio. For the 1993–2022 time mean temperature along PX40, the sloping shape of the steep vertical temperature gradient in the Kuroshio (Figure 6b) coincided with, and was replicated by, the sloping shape of the strong warming trend in the Kuroshio (Figure 6a). However, because the largest Kuroshio temperature trends at PX40 (around 141.8°E and 420-m deep) do not coincide with the steepest vertical temperature gradients (Figures 6a and 6b), we hypothesize that additional factors likely also contribute to the observed subsurface warming trends in the Kuroshio at PX40.

### 3.2. Trends in Marine Heatwave Occurrence

Over the 30-year time series, a positive trend in the number of MHW days per year was observed throughout the water column from close to the coast out to around 146.5°E (Figure 7a). This trend was significant within the Kuroshio, between 139.9°E and 142.9°E, increasing by as much as 4.2 days per year. If these significant trends are maintained through to the end of the century (i.e., 2100) then, relative to the 1993–2022 baseline and threshold used here, the number of subsurface Kuroshio MHW days per year at PX40 would increase by between 120 and

330 days. Similar increases in surface MHW days per year, relative to a fixed historical (1981–2005) threshold, are projected for this same region and same future time period using a high-resolution ocean model (Kawakami et al., 2024). Further offshore, east of 146.5°E, the observed 30-year trend in MHW days per year at PX40 became weakly negative and was not significant (Figure 7a).

Long-term changes in MHWs can be caused by changes in the temperature mean and/or temperature variability. Here, as in many other MHW studies (e.g., Du et al., 2022; Kawakami et al., 2024; Oliver, 2019; Oliver et al., 2018, 2019), trends (or lack thereof) in the number of MHW days per year were largely due to trends in ocean temperature causing a change in the mean temperature. In particular, the significant Kuroshio warming trend occurred in the same location (139.9°E–142.9°E) as the significant increase in the number of MHW days per year (Figures 6a and 7a). In contrast, there were no significant increasing trends in MHW days per year when the temperature trend was removed before identifying MHWs (Figure 7b). In fact, a significant decrease in the number of MHW days per year (reaching as large as −2 days per year) was instead found between 140.8°E and 142.3°E. This decrease in MHW days at the offshore edge of the Kuroshio was likely due to the decreased variability here during the second half of the time series compared to the first half (Figure S1a in Supporting Information S1). Decreases in variance were also evident (Figure S1b in Supporting Information S1) in both daily SLA (comparing 1993–2007 with 2008–2022) and monthly GLORYS depth-integrated velocity eddy kinetic energy (comparing 1993–2007 with 2008–2020). We suspect this decreased variability may be related to fluctuations in wind forcing over the interior North Pacific Ocean that influence the dynamic state of the Kuroshio-Kuroshio Extension system (e.g., Qiu et al., 2014). Trends in MHW days per year were not significant elsewhere along the transect when using the detrended temperature anomaly time series (Figure 7b).

Due to the influence of the Kuroshio warming trend on MHW identification and occurrence, the synthetic temperature time series were detrended before identifying MHWs for the analyses in the following sections (Sections 3.3 and 3.4). Detrending allowed us to examine the influence of other physical processes independent of this long-term background warming.

### 3.3. Marine Heatwave Primary Metrics

Reporting of standardized MHW metrics helps facilitate comparisons between different events, locations, and times (Hobday et al., 2016). Here, we present the primary MHW metrics of intensity and duration averaged over all events between 1993 and 2022. As noted above, the synthetic temperature anomaly time series were detrended before identifying the MHWs from which these primary metrics were computed.

At every longitude along the transect, the largest mean event intensities were found below the sea surface (Figure 8a). Similar subsurface intensification has been observed by studies examining subsurface MHWs in the tropical western Pacific Ocean (Hu et al., 2021) and coastal southeastern Australia (Schaeffer & Roughan, 2017). Along PX40, the largest mean event intensities (4.1°C) occurred around 500-m deep at approximately 145°E (Figure 8a). This longitude coincides with where the Kuroshio Extension meanders most closely to PX40 (Figures 1 and 2). Variability in the position of the Kuroshio Extension, which is known to be sizeable in this region (Donohue et al., 2010; Qiu et al., 2014), likely drives these large mean event intensities at 145°E.

Mean event durations (Figure 8b) followed a different pattern than mean event intensities (Figure 8a). The shortest mean durations (13.3 days) were found at the western boundary, consistent with the shorter durations that are typical of surface MHWs in WBC regions (Holbrook et al., 2019; Sen Gupta et al., 2020). Mean MHW durations then increased moving east along the transect, with the longest mean durations (35.5 days) occurring around 144°E at depths below 400-m (Figure 8b). MHWs at this depth are most likely advection-driven by Kuroshio Extension variability (e.g., Xu et al., 2024), and we hypothesize that strengthening of the Kuroshio Extension could be a key driver of the longer MHW durations here. Indeed, when averaging monthly GLORYS depth-integrated velocities for the longest (>30-day) duration events over 1993–2020 at 144.05°E and 440-m deep (i.e., the grid point along the transect where mean event duration was longest), the Kuroshio, Kuroshio Extension, and first quasi-stationary meander recirculation were all significantly stronger than in the mean state (Figure S2 in Supporting Information S1). Further east along the transect, mean event durations tended to decrease again (Figure 8b).

Longer mean durations were also evident near the surface (shallower than 250-m) around 148°E. We are unsure of what unique physical processes maybe driving the increased MHW duration in this region compared to elsewhere

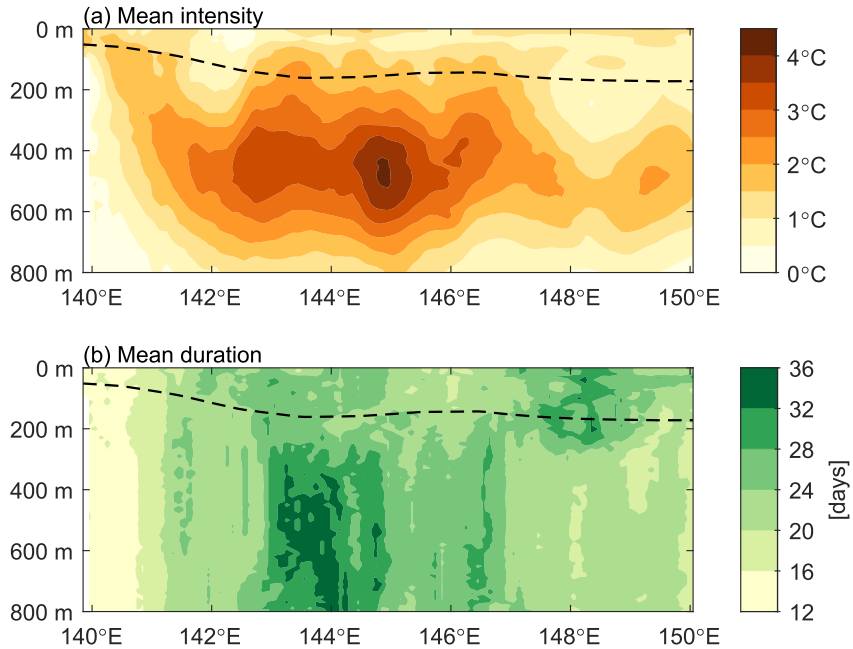


**Figure 8.** Mean (a) intensity and (b) duration averaged over all marine heatwave events between 1993 and 2022. The black dashed line is the maximum climatological mixed layer depth.

in the near-surface. However, this region coincides with where the synthetic temperature anomaly time series most poorly reproduced observed temperature variability (Figures 4c and 5c). The increased mean duration (and slightly decreased mean intensity) at this location may therefore reflect limitations in the method's ability to reproduce temperature variability in the surface mixed layer to a high degree of accuracy (see also Willis et al., 2003).

### 3.4. Influence of ENSO on Marine Heatwave Occurrence

Due to the 90th percentile temperature anomaly threshold, MHW conditions were experienced during 10% of the study time period. However, MHW conditions could be experienced for different percentages of time during each individual ENSO phase (i.e., El Niño, La Niña, and neutral periods). Indeed, MHW conditions would only occur around 10% of the time during each ENSO phase if ENSO did not influence MHW occurrence.

Surface MHW occurrence along PX40 was not significantly different from this 10% occurrence rate (Figures 9a and 9c), consistent with the weak correlation between the Niño 3.4 index and SST in this region (e.g., Talley et al., 2011). Holbrook et al. (2019), Sen Gupta et al. (2020), and Gregory et al. (2024) also show essentially no relationship between ENSO and surface MHW occurrence in the PX40 region east of Japan. The analyses in this section therefore focus on the subsurface as, in contrast to the surface, subsurface MHW occurrence along PX40 demonstrated a strong relationship with ENSO (Figure 9). Relying only on SST observations would thus lead to incomplete conclusions being drawn about the influence of ENSO on MHW occurrence along this transect.

During El Niño, subsurface MHWs along PX40 occurred significantly more often in a western region between approximately 141.4°E and 144.6°E and an eastern region between approximately 147.5°E and 148.6°E (Figures 9a and 9b). At both locations, the increased MHW occurrence was evident from the base of the surface mixed layer down to 800-m deep. In contrast, subsurface MHWs during La Niña occurred significantly less often between approximately 144°E and 146.6°E and from approximately 147.6°E out to the eastern end of the transect (Figures 9c and 9d). This decreased MHW occurrence was also typically evident from the base of the surface mixed layer down to 800-m deep, although there were some regions where it did not extend all the way up to the base of the surface mixed layer.

Recently, Wang et al. (2024) demonstrated that surface and near-surface velocities in the Kuroshio and Kuroshio Extension strengthen during El Niño due to a strengthening of the midlatitude westerlies driving a more negative

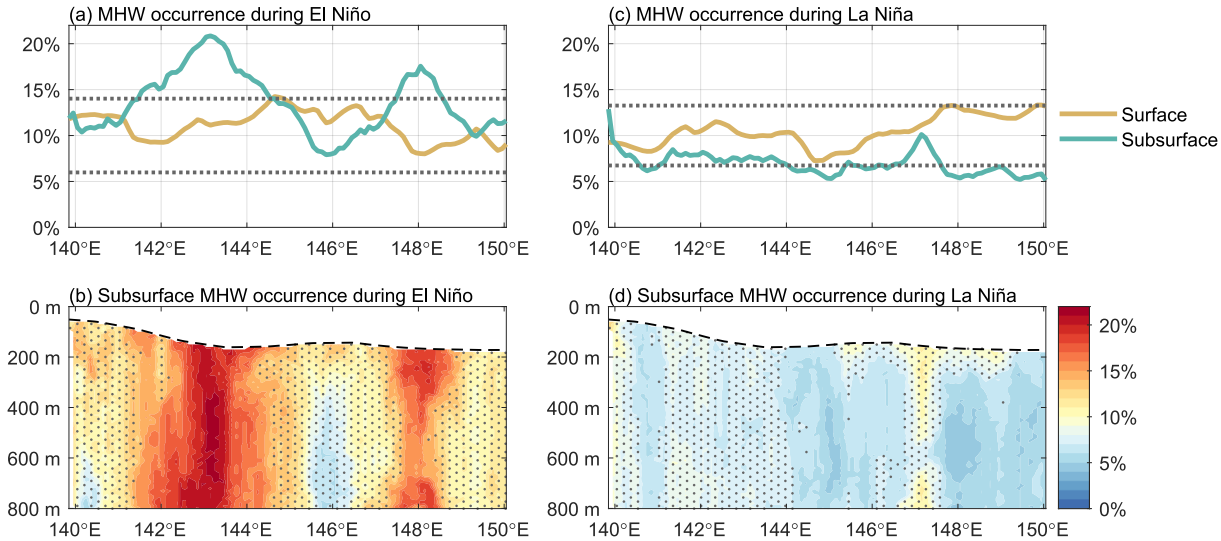


**Figure 9.** Percentage of time that marine heatwaves (MHWs) occurred along PX40 during (a and b) El Niño and (c and d) La Niña over the 1993–2022 time period. (a and c) MHW occurrence depth-averaged below the maximum climatological mixed layer depth (subsurface, green) and at the surface from sea surface temperature observations (surface, brown). Dotted lines bound where occurrence is not significantly different from 10% of the time at the 95% significance level. (b and d) MHW occurrence below the maximum climatological mixed layer depth (black dashed line). Stippling is where occurrence is not significantly different from 10% of the time at the 95% significance level.

wind stress curl over the subtropical North Pacific Ocean. Given that the strength of the Kuroshio Extension and its southern recirculation gyre tend to vary roughly in phase (Qiu et al., 2014), we may expect both to strengthen during El Niño periods. Indeed, using the GLORYS eddy-resolving ocean reanalysis, both the Kuroshio Extension and its southern recirculation gyre were found to strengthen during El Niño (Figure 10b), thereby transporting more warm subtropical-origin water. Mean subsurface temperatures along PX40 were therefore warmer during El Niño, compared to the 1993–2022 time mean, where the strengthened southern recirculation gyre intersected the transect (Figure 11a). These warmer mean temperatures led to the increased subsurface MHW occurrence observed in both regions along the transect (141.4°E–144.6°E and 147.5°E–148.6°E) during El Niño (Figures 9b and 11a).

The stronger Kuroshio Extension and southern recirculation gyre during El Niño were also associated with a more coherent (less variable) Kuroshio Extension jet (Figure 10), consistent with the inverse relationship between Kuroshio Extension strength and path length shown by Qiu et al. (2014). Reduced variability in the path of the Kuroshio Extension resulted in reduced temperature variability along PX40 between 142.1°E and 148.1°E during El Niño periods compared to the full 1993–2022 time period (Figure 11b). Decreased variance produces a narrower distribution of temperature anomalies and therefore less extreme values. Between approximately 144.6°E and 147.5°E, the reduction in temperature variability during El Niño (Figure 11b) was substantial enough to oppose the positive shift in the temperature anomaly distribution driven by the increase in mean temperature during El Niño (Figure 11a). The net result was no significant change in subsurface MHW occurrence at this location (144.6°E–147.5°E) along the transect (Figure 9b).

Changes in subsurface MHW occurrence along PX40 during La Niña did not mirror changes during El Niño (Figure 9). During La Niña, the Kuroshio Extension and its southern recirculation gyre were both weaker (Figure 10c), resulting in reduced transport of warm subtropical-origin water and, importantly, reduced recirculation of this warm water across PX40. Slightly cooler mean subsurface temperatures, compared to the 1993–2022 time mean, were therefore found along much of PX40 (Figure 11c). The path of the Kuroshio Extension also appeared to be less tightly defined (more variable) during La Niña, resulting in a more diffuse mean state of the Kuroshio Extension (Figure 10). Decreases in subsurface MHW occurrence along PX40 during La Niña therefore tended to be found where there were compounding effects of a decrease in both mean temperature and temperature variability compared to the full 1993–2022 time period (Figures 11c and 11d). This slight negative shift and slight narrowing of the temperature anomaly distribution combined to produce less extreme positive temperature anomalies.

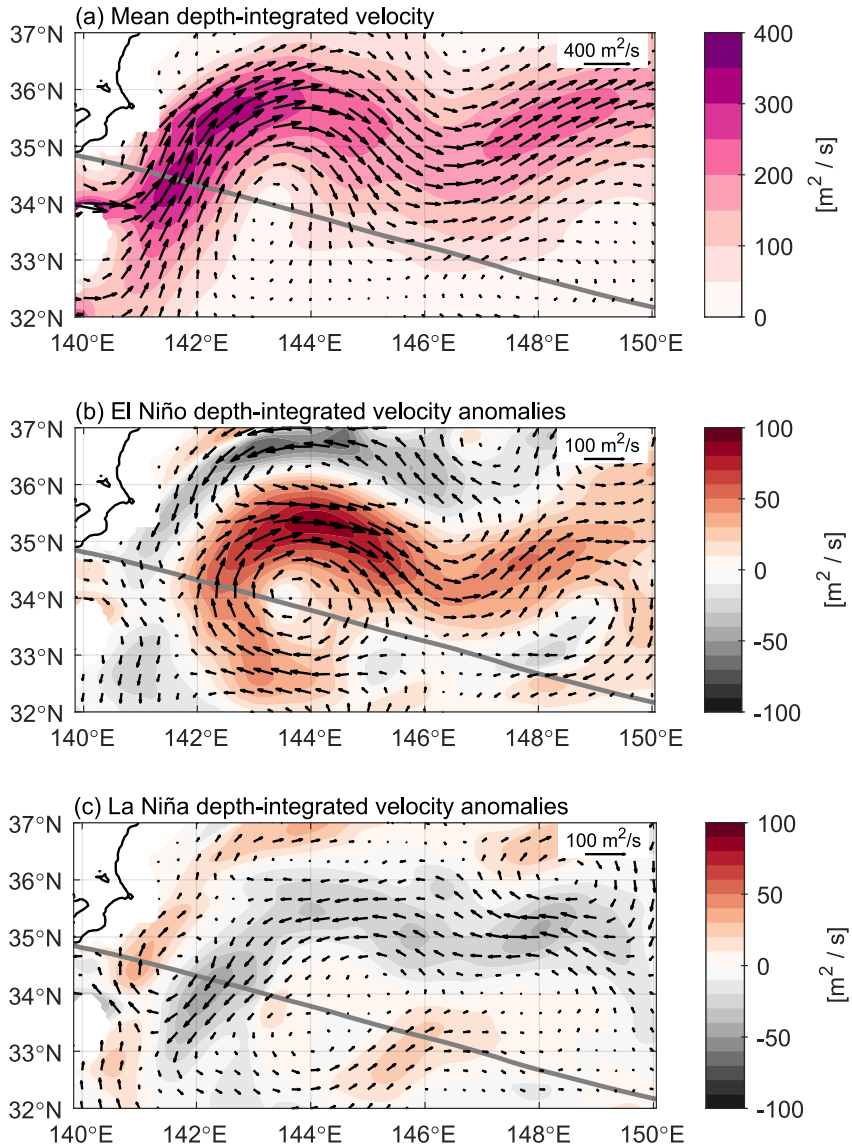


**Figure 10.** Monthly GLORYS 0–800-m depth-integrated velocity (a) 1993–2020 time mean, and anomalies averaged during (b) El Niño and (c) La Niña. Scale arrows are in the top right of each panel, but note the different scale for (a) compared to (b) and (c). The thick gray line is PX40. The black contour is the Japan coastline (0-m isobath).

When considering El Niño diversity (Capotondi et al., 2015), similar increases in subsurface MHW occurrence were found along PX40 irrespective of whether central Pacific or eastern Pacific El Niño conditions existed (Figure 12). However, the increase in subsurface MHW occurrence was significant over a larger area of the PX40 cross-section during central Pacific El Niño conditions than during eastern Pacific El Niño conditions. These differences likely arise because, although central Pacific and eastern Pacific El Niño conditions both drive strengthening of the Kuroshio and Kuroshio Extension, the strengthening is typically greater during a central Pacific El Niño than an eastern Pacific El Niño (Wang et al., 2024).

In this study, we defined MHWs as events where temperature anomalies were above the 90th percentile threshold for at least 10 days. However, our results are rather insensitive to the choice of duration threshold. When using a 20-day duration threshold, subsurface MHWs occurred significantly more often than expected during El Niño in the same regions along PX40 as for the 10-day duration threshold (Figure S3a in Supporting Information S1). Likewise, subsurface MHW occurrence was reduced during La Niña periods, although significant over a substantially smaller cross-sectional area of the transect when using a 20-day duration threshold compared with the

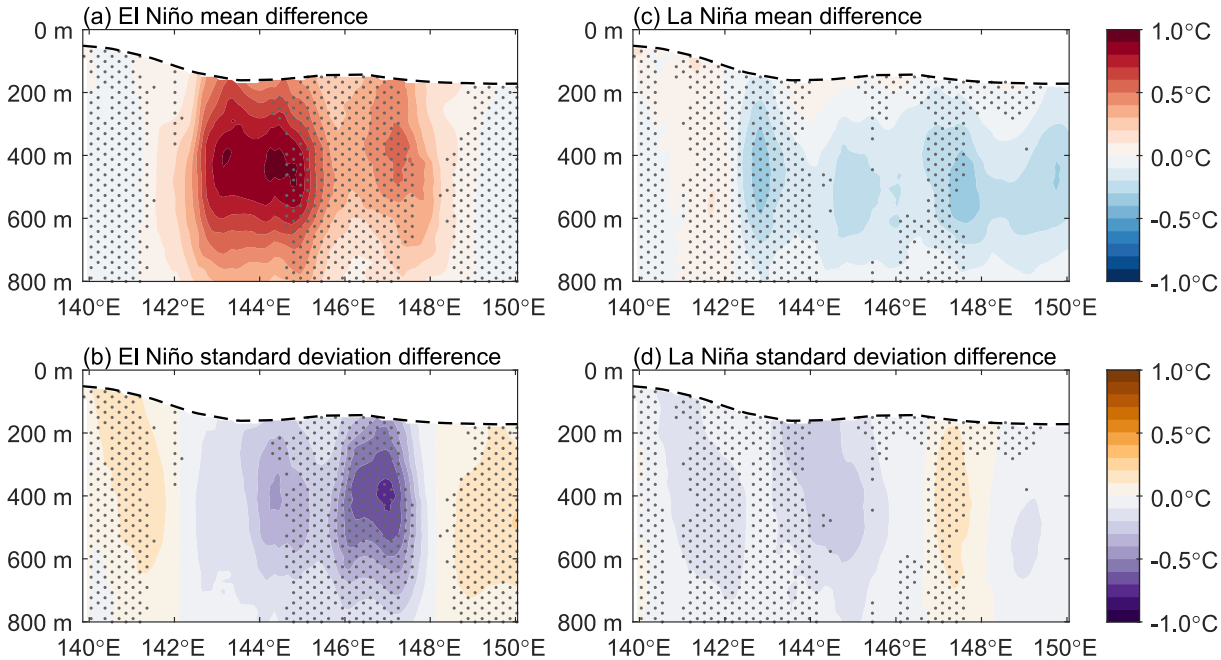


**Figure 11.** Difference in temperature anomaly (a and c) mean and (b and d) standard deviation between (a and b) El Niño compared to the full 1993–2022 time series (red indicates warmer temperatures and purple indicates smaller standard deviations during El Niño) and (c and d) La Niña compared to the full 1993–2022 time series (blue indicates cooler temperatures and purple indicates smaller standard deviations during La Niña). Stippling is where MHW occurrence below the maximum climatological mixed layer depth (black dashed line) is not significantly different from 10% of the time at the 95% significance level (see Figure 9).

10-day duration threshold (Figure S3b in Supporting Information S1). Surface MHWs along PX40 did not occur at a significantly different rate than expected during El Niño or La Niña when using a 20-day duration threshold, nor when the Hobday et al. (2016) definition was applied to daily SST observations (Figure S4 in Supporting Information S1). For these different duration thresholds, MHWs no longer occurred during 10% of the study

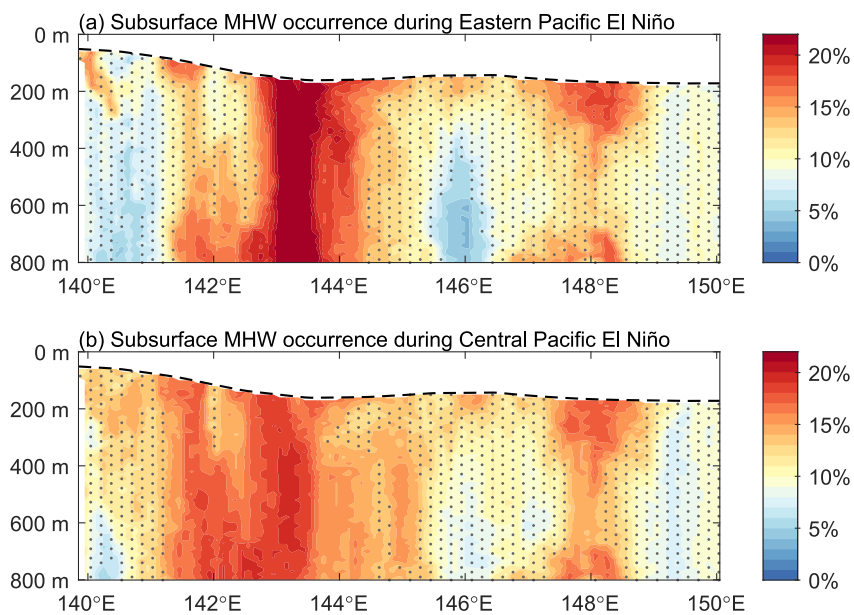


**Figure 12.** Percentage of time that subsurface marine heatwaves (MHWs) occurred along PX40 during (a) eastern Pacific El Niño conditions (identified using the Niño 3 index) and (b) central Pacific El Niño conditions (identified using the Niño 4 index) over 1993–2022. The black dashed line is the maximum climatological mixed layer depth. Stippling is where occurrence is not significantly different from 10% of the time at the 95% significance level.

period. Therefore, 95% confidence intervals were assessed using a Monte Carlo approach (with $1 \times 10^4$ iterations) where the start dates of observed MHW events were randomly assigned (observed durations and intensities were retained).

## 4. Conclusions

Here, we have produced a novel 30-year time series of synthetic subsurface temperature anomalies at the western end of an HR-XBT transect that intersects the Kuroshio and Kuroshio Extension east of Japan. This time series has a 10-day temporal resolution, representing the 10-day average temperature. MHWs were defined as events where the temperature anomaly was above the 90th percentile. All identified MHW events were therefore at least 10 days long. Nevertheless, our conclusions are rather insensitive to the duration threshold used to identify MHWs. The largest mean MHW event intensities were found to occur in the subsurface at every longitude along the transect, with the strongest mean intensity signal associated with variability in the path of a Kuroshio Extension meander around 145°E. At the western edge of the transect, in the Kuroshio, the number of MHW days per year significantly increased between 1993 and 2022. This increase in Kuroshio MHW days was caused by a significant subsurface warming trend in the Kuroshio, which appears to be predominantly driven by heaving of isotherms (e.g., Liu et al., 2021). When using the detrended temperature anomaly time series to identify MHWs, ENSO was found to influence the occurrence of subsurface MHWs along PX40. During El Niño, a more negative wind stress curl over the subtropical North Pacific Ocean (Wang et al., 2024) strengthens the Kuroshio Extension and its southern recirculation gyre, thereby producing warmer mean subsurface temperatures where the current intersects the transect. As such, subsurface MHWs occurred significantly more often during El Niño periods where the strengthened southern recirculation gyre of the Kuroshio Extension intersected the transect. This increase in subsurface MHW occurrence was broadly similar under both central Pacific and eastern Pacific El Niño conditions. Subsurface MHWs along PX40 occurred less often during La Niña periods.

Despite influencing subsurface MHW occurrence, ENSO did not significantly influence the occurrence of surface MHWs along the transect. MHW occurrence at the sea surface during El Niño and La Niña therefore differed from that below the surface mixed layer, reflecting different forcing mechanisms (e.g., Elzahaby et al., 2021; Großelindemann et al., 2022; Xu et al., 2024). These differences at PX40 further emphasize that both surface and subsurface observations are needed to fully understand MHW events and their impacts. In practice, subsurface MHW identification is often not feasible as the sufficiently long time series required to identify MHWs are rare in the subsurface, and SST alone is not representative of temperatures below the surface mixed layer. Yet HR-XBT transects provide long-term observations of temperature between the surface and 800-m deep in all major ocean basins (Goni et al., 2019). The method used in this study could thus be implemented to evaluate subsurface MHW properties along these other HR-XBT transects. However, WBCs typically extend much deeper than 800-m (Chandler et al., 2022a; Zilberman et al., 2023). Because of the deep-reaching influence of the Kuroshio Extension (e.g., Chandler et al., 2022a), we think it likely that the warmer subsurface temperatures and increased subsurface MHW occurrence observed along PX40 during El Niño will also extend much deeper than 800-m and possibly as deep as 5,000-m (e.g., Jayne et al., 2009).

The insignificant influence of ENSO on surface MHW occurrence along PX40 reflects the weak influence ENSO has on SST here (e.g., Talley et al., 2011). However, north of PX40, starting around 36°N, ENSO has a much stronger influence on SST. Cold SST anomalies occur during El Niño, driven by a deeper Aleutian Low and stronger midlatitude westerlies (Wang et al., 2024), with warm SST anomalies during La Niña. Nevertheless, the potential subsurface response in this northern region is unclear. ENSO predominantly drives a change in the strength of the Kuroshio Extension and its southern recirculation gyre, rather than a meridional shift of the system. That being said, the Kuroshio Extension was typically a more defined jet during El Niño periods, with less transport occurring north of approximately 36°N. Less warm subtropical-origin water would therefore be transported further north, which would be expected to decrease subsurface MHW occurrence. On the other hand, the Kuroshio and Kuroshio Extension are both generally weaker during La Niña (Figure 10c; Wang et al., 2024), which would also result in reduced transport of warm subtropical-origin water. The dominant influence on subsurface MHW occurrence in this northern region may instead stem from anticyclonic (warm-core) eddies spawned from the Kuroshio Extension (e.g., Elzahaby & Schaeffer, 2019; Großelindemann et al., 2022; Xu et al., 2024; Zhang et al., 2023). The potential impact of these eddies on subsurface MHWs north of PX40 is yet to be explored.

This work has demonstrated that variability in the Kuroshio-Kuroshio Extension system exerts a strong control on subsurface temperature, and therefore subsurface MHW occurrence, along PX40. Due to the length of our novel 30-year synthetic temperature time series, we have largely focused on the influence of ENSO. Yet other modes of climate variability, such as the PDO, also exhibit a relationship with the dynamics of the Kuroshio-Kuroshio Extension system. During a positive PDO, the westerly winds over the North Pacific Ocean tend to be stronger and located further south (Talley et al., 2011). As such, the phase of the PDO can influence, for example, the strength of the Kuroshio (e.g., Wang et al., 2016) and SST anomalies in the Kuroshio-Oyashio Extension region (e.g., Newman et al., 2016; Zhou et al., 2024). We therefore hypothesize that the PDO may also influence subsurface MHW occurrence along PX40. Due to the canonically multidecadal periodicity of the PDO (as opposed to the interannual periodicity of ENSO), its impact on subsurface MHW occurrence along this transect has not been examined here and remains unknown. However, over the time period covered by our study, a partial correlation analysis (i.e., correlating annually low-pass filtered subsurface temperature anomalies and ENSO while controlling for the PDO, and correlating annually low-pass filtered subsurface temperature anomalies and the PDO while controlling for ENSO) demonstrated that subsurface temperature anomalies along PX40 were more strongly correlated with ENSO than with the PDO (Text S2 in Supporting Information S1).

Lastly, present-day climate models struggle to predict the occurrence of monthly MHWs in the Kuroshio Extension (Zhou et al., 2024). This limited predictive skill is likely due to the coarser spatial resolution ($\geq 1/4°$) of these models (Hayashida et al., 2020; Zhou et al., 2024). As such, there is limited lead time to prepare for extreme ocean temperature events. Yet subsurface ocean temperatures can have a significant influence on fisheries in the Kuroshio-Kuroshio Extension region (e.g., Noto & Yasuda, 1999; Yatsu, 2019). Knowledge that, along PX40, subsurface temperatures increase and subsurface MHWs occur more often during El Niño periods should enhance MHW predictability in this region and thus aid in designing and implementing MHW adaptation plans (e.g., Pershing et al., 2018).

## Data Availability Statement

HR-XBT data from transect PX40 were made available by the Scripps Institution of Oceanography HR-XBT program (https://www-hrx.ucsd.edu/px40.html). The World Ocean Atlas 2023 temperature climatology was obtained from NOAA NCEI at https://doi.org/10.25921/va26-hv25 (Reagan et al., 2024). Sea surface height data (SLA and ADT) were obtained from the EU Copernicus Marine Service at https://doi.org/10.48670/moi-00148 (CMEMS, 2024a). Sea surface temperature data were obtained from NOAA NCEI at https://doi.org/10.25921/RE9P-PT57 (Huang et al., 2024). Data from the Kuroshio Extension System Study were provided by Kathleen Donohue and can be accessed through the program website at https://uskess.whoi.edu/overview/dataproducts/. Bathymetry was from the 15 arc second GEBCO 2023 gridded bathymetry product (GEBCO Compilation Group, 2023). The mixed layer depth climatology can be accessed at https://doi.org/10.17882/91774 (de Boyer Montégut, 2023). The Oceanic Niño Index (https://www.cpc.ncep.noaa.gov/data/indices/oni.ascii.txt) and Niño 3 and Niño 4 indices (https://www.cpc.ncep.noaa.gov/data/indices/ersst5.nino.mth.91-20.ascii) were all obtained from NOAA CPC at https://www.cpc.ncep.noaa.gov/data/indices/. GLORYS12V1 velocity data were obtained from the EU Copernicus Marine Service at https://doi.org/10.48670/moi-00021 (CMEMS, 2024b). Cross-transect geostrophic velocity for transect PX40 can be accessed at https://doi.org/10.5281/zenodo.5851311 (Chandler et al., 2022b). Dates of the Kuroshio large meander events were obtained from JMA at https://www.data.jma.go.jp/gmd/kaiyou/data/shindan/b_2/kuroshio_stream/kuroshio_stream.html. The Dipole Mode Index was obtained from NOAA OSMC at https://stateoftheocean.osmc.noaa.gov/sur/ind/dmi.php. ERA5 relative vorticity data were obtained from the EU Copernicus Climate Change Service Climate Data Store at https://doi.org/10.24381/cds.6860a573 (Hersbach et al., 2023). Color maps are from BrewerMap (https://github.com/DrosteEffect/BrewerMap). This work utilized some functions from the MATLAB Climate Data Toolbox (Greene et al., 2019). The objectively mapped HR-XBT observations and the synthetic temperature anomaly time series from this study are permanently and publicly available at https://doi.org/10.5281/zenodo.14219180 (Chandler, 2024). The MATLAB script used to produce the synthetic temperature time series is also available through the above Zenodo link, as are implementations of the script in Julia and in R (Chandler, 2024).

**Acknowledgments**
We would like to thank the crews of the ships that collected these HR-XBT measurements (JRS Canis, Tacoma Trader, Cape Franklin, Undarum, and Tallahassee), and Kathleen Donohue for providing the Kuroshio Extension System Study data. We also thank the editor and anonymous reviewers for their time and the feedback they provided on earlier versions of this manuscript. The HR-XBT program data collection was supported by the NOAA Global Ocean Monitoring and Observing Program through Award NA20OAR4320278. MC, JS, and NZ were also supported by the NOAA Global Ocean Monitoring and Observing Program through Award NA20OAR4320278. MC completed revisions on this manuscript while employed as a postdoctoral researcher by The Wilderness Society.

## References

Ando, K., Lin, X., Villanoy, C., Danchenkov, M., Lee, J.-H., He, H.-J., et al. (2021). Half-century of scientific advancements since the cooperative study of the Kuroshio and adjacent regions (CSK) programme—Need for a new Kuroshio research. *Progress in Oceanography*, *193*, 102513. https://doi.org/10.1016/j.pocean.2021.102513

Bond, N. A., & Cronin, M. F. (2008). Regional weather patterns during anomalous air–sea fluxes at the Kuroshio Extension Observatory (KEO). *Journal of Climate*, *21*(8), 1680–1697. https://doi.org/10.1175/2007JCLI1797.1

Cai, L., Xu, L., Tang, D., Shao, W., Liu, Y., Zuo, J., & Ji, Q. (2020). The effects of ocean temperature gradients on bigeye tuna (*Thunnus obesus*) distribution in the equatorial eastern Pacific Ocean. *Advances in Space Research*, *65*(12), 2749–2760. https://doi.org/10.1016/j.asr.2020.03.030

Capotondi, A., Wittenberg, A. T., Newman, M., Di Lorenzo, E., Yu, J.-Y., Braconnot, P., et al. (2015). Understanding ENSO diversity. *Bulletin of the American Meteorological Society*, *96*(6), 921–938. https://doi.org/10.1175/BAMS-D-13-00117.1

Cavole, L., Demko, A., Diner, R., Giddings, A., Koester, I., Pagniello, C., et al. (2016). Biological impacts of the 2013–2015 warm-water anomaly in the Northeast Pacific: Winners, losers, and the future. *Oceanography*, *29*(2). https://doi.org/10.5670/oceanog.2016.32

Chandler, M. (2024). Data in support of "ENSO influences subsurface marine heatwave occurrence in the Kuroshio Extension" [Dataset]. *Zenodo*. https://doi.org/10.5281/zenodo.14219180

Chandler, M., Zilberman, N. V., & Sprintall, J. (2022a). Seasonal to decadal Western boundary current variability from sustained ocean observations. *Geophysical Research Letters*, *49*(12), e2022GL097834. https://doi.org/10.1029/2022GL097834

Chandler, M., Zilberman, N. V., & Sprintall, J. (2022b). Seasonal to decadal Western boundary current variability from sustained ocean observations [Dataset]. *Zenodo*. https://doi.org/10.5281/ZENODO.5851312

CMEMS. (2024a). Global ocean gridded L4 sea surface heights and derived variables reprocessed 1993–Ongoing [Dataset]. *EU Copernicus Marine Service Information Marine Data Store*. https://doi.org/10.48670/MOI-00148

CMEMS. (2024b). Global ocean physics reanalysis [Dataset]. *EU Copernicus Marine Service Information Marine Data Store*. https://doi.org/10.48670/MOI-00021

de Boyer Montégut, C. (2023). Mixed layer depth climatology computed with a density threshold criterion of 0.03 kg/m3 from 10 m depth value [Dataset]. *SEANOE*. https://doi.org/10.17882/91774

de Boyer Montégut, C., Madec, G., Fischer, A. S., Lazar, A., & Iudicone, D. (2004). Mixed layer depth over the global ocean: An examination of profile data and a profile-based climatology. *Journal of Geophysical Research*, *109*(C12). https://doi.org/10.1029/2004JC002378

Donohue, K. A., Watts, D. R., Tracey, K. L., Greene, A. D., & Kennelly, M. (2010). Mapping circulation in the Kuroshio extension with an array of current and pressure recording inverted echo sounders. *Journal of Atmospheric and Oceanic Technology*, *27*(3), 507–527. https://doi.org/10.1175/2009JTECHO686.1

Draper, N. R., & Smith, H. (1998). *Applied regression analysis* (3rd ed.), John Wiley & Sons. https://doi.org/10.1002/9781118625590

Du, Y., Feng, M., Xu, Z., Yin, B., & Hobday, A. J. (2022). Summer marine heatwaves in the Kuroshio-Oyashio extension region. *Remote Sensing*, *14*(13), 2980. https://doi.org/10.3390/rs14132980

Elzahaby, Y., & Schaeffer, A. (2019). Observational insight into the subsurface anomalies of marine heatwaves. *Frontiers in Marine Science*, *6*, 745. https://doi.org/10.3389/fmars.2019.00745

Elzahaby, Y., Schaeffer, A., Roughan, M., & Delaux, S. (2021). Oceanic circulation drives the deepest and longest marine heatwaves in the east Australian current system. *Geophysical Research Letters*, *48*(17), e2021GL094785. https://doi.org/10.1029/2021GL094785

Emery, W. J., & Thomson, R. E. (2001). *Data analysis methods in physical oceanography* (2nd ed.), Elsevier.

Farchadi, N., McDonnell, L. H., Ryan, S., Lewison, R. L., & Braun, C. D. (2025). Marine heatwaves are in the eye of the beholder. *Nature Climate Change*, *15*(3), 236–239. https://doi.org/10.1038/s41558-025-02257-6

Fujioka, K., Fukuda, H., Furukawa, S., Tei, Y., Okamoto, S., & Ohshimo, S. (2018). Habitat use and movement patterns of small (age-0) juvenile Pacific Bluefin tuna (Thunnus orientalis) relative to the Kuroshio. *Fisheries Oceanography*, *27*(3), 185–198. https://doi.org/10.1111/fog.12244

GEBCO Compilation Group. (2023). GEBCO 2023 grid [Dataset]. https://doi.org/10.5285/f98b053b-0cbc-6c23-e053-6c86abc0af7b

Gilson, J., Roemmich, D., Cornuelle, B., & Fu, L.-L. (1998). Relationship of TOPEX/Poseidon altimetric height to steric height and circulation in the North Pacific. *Journal of Geophysical Research*, *103*(C12), 27947–27965. https://doi.org/10.1029/98JC01680

Goni, G. J., Sprintall, J., Bringas, F., Cheng, L., Cirano, M., Dong, S., et al. (2019). More than 50 years of successful continuous temperature section measurements by the global expendable bathythermograph network, its integrability, societal benefits, and future. *Frontiers in Marine Science*, *6*, 452. https://doi.org/10.3389/fmars.2019.00452

Greene, C. A., Thirumalai, K., Kearney, K. A., Delgado, J. M., Schwanghart, W., Wolfenbarger, N. S., et al. (2019). The climate data toolbox for MATLAB. *Geochemistry, Geophysics, Geosystems*, *20*(7), 3774–3781. https://doi.org/10.1029/2019GC008392

Gregory, C. H., Artana, C., Lama, S., León-FonFay, D., Sala, J., Xiao, F., et al. (2024). Global marine heatwaves under different flavors of ENSO. *Geophysical Research Letters*, *51*(20), e2024GL110399. https://doi.org/10.1029/2024GL110399

Großelindemann, H., Ryan, S., Ummenhofer, C. C., Martin, T., & Biastoch, A. (2022). Marine heatwaves and their depth structures on the Northeast U.S. Continental shelf. *Frontiers in Climate*, *4*, 857937. https://doi.org/10.3389/fclim.2022.857937

Hayashida, H., Matear, R. J., Strutton, P. G., & Zhang, X. (2020). Insights into projected changes in marine heatwaves from a high-resolution ocean circulation model. *Nature Communications*, *11*(1), 4352. https://doi.org/10.1038/s41467-020-18241-x

Hersbach, H., Bell, B., Berrisford, P., Biavati, G., Horányi, A., Muñoz Sabater, J., et al. (2023). ERA5 monthly averaged data on pressure levels from 1940 to present [Dataset]. *Copernicus Climate Change Service Climate Data Store*. https://doi.org/10.24381/cds.6860a573

Hobday, A. J., Alexander, L. V., Perkins, S. E., Smale, D. A., Straub, S. C., Oliver, E. C. J., et al. (2016). A hierarchical approach to defining marine heatwaves. *Progress in Oceanography*, *141*, 227–238. https://doi.org/10.1016/j.pocean.2015.12.014

Holbrook, N. J., Scannell, H. A., Sen Gupta, A., Benthuysen, J. A., Feng, M., Oliver, E. C. J., et al. (2019). A global assessment of marine heatwaves and their drivers. *Nature Communications*, *10*(1), 2624. https://doi.org/10.1038/s41467-019-10206-z

Hu, S., Li, S., Zhang, Y., Guan, C., Du, Y., Feng, M., et al. (2021). Observed strong subsurface marine heatwaves in the tropical Western Pacific Ocean. *Environmental Research Letters*, *16*(10), 104024. https://doi.org/10.1088/1748-9326/ac26f2

Huang, B., Liu, C., Banzon, V., Freeman, E., Graham, G., Hankins, B., et al. (2021). Improvements of the Daily Optimum Interpolation Sea Surface Temperature (DOISST) version 2.1. *Journal of Climate*, *34*(8), 2923–2939. https://doi.org/10.1175/JCLI-D-20-0166.1

Huang, B., Liu, C., Banzon, V. F., Freeman, E., Graham, G., Hankins, W., et al. (2024). NOAA 0.25-degree Daily Optimum Interpolation Sea Surface Temperature (OISST), version 2.1 [Dataset]. *NOAA National Centers for Environmental Information*. https://doi.org/10.25921/RE9P-PT57

Jacox, M. G., Alexander, M. A., Amaya, D., Becker, E., Bograd, S. J., Brodie, S., et al. (2022). Global seasonal forecasts of marine heatwaves. *Nature*, *604*(7906), 486–490. https://doi.org/10.1038/s41586-022-04573-9

Jacox, M. G., Alexander, M. A., Bograd, S. J., & Scott, J. D. (2020). Thermal displacement by marine heatwaves. *Nature*, *584*(7819), 82–86. https://doi.org/10.1038/s41586-020-2534-z

Jayne, S. R., Hogg, N. G., Waterman, S. N., Rainville, L., Donohue, K. A., Randolph Watts, D., et al. (2009). The Kuroshio extension and its recirculation gyres. *Deep Sea Research Part I: Oceanographic Research Papers*, *56*(12), 2088–2099. https://doi.org/10.1016/j.dsr.2009.08.006

Kawabe, M. (1985). Sea level variations at the Izu Islands and typical stable paths of the Kuroshio. *Journal of the Oceanographical Society of Japan*, *41*(5), 307–326. https://doi.org/10.1007/BF02109238

Kawabe, M. (1995). Variations of current path, velocity, and volume transport of the Kuroshio in relation with the large meander. *Journal of Physical Oceanography*, *25*(12), 3103–3117. https://doi.org/10.1175/1520-0485(1995)025⟨3103:VOCPVA⟩2.0.CO;2

Kawakami, Y., Nakano, H., Urakawa, L. S., Toyoda, T., Sakamoto, K., Nishikawa, S., et al. (2024). Future changes in marine heatwaves based on high-resolution ensemble projections for the northwestern Pacific Ocean. *Journal of Oceanography*, *80*(3), 177–195. https://doi.org/10.1007/s10872-024-00714-y

Kitagawa, T., Kato, Y., Miller, M. J., Sasai, Y., Sasaki, H., & Kimura, S. (2010). The restricted spawning area and season of Pacific Bluefin tuna facilitate use of nursery areas: A modeling approach to larval and juvenile dispersal processes. *Journal of Experimental Marine Biology and Ecology*, *393*(1), 23–31. https://doi.org/10.1016/j.jembe.2010.06.016

Lellouche, J.-M., Greiner, E., Bourdallé-Badie, R., Garric, G., Melet, A., Drévillon, M., et al. (2021). The Copernicus Global 1/12° Oceanic and Sea ice GLORYS12 reanalysis. *Frontiers in Earth Science*, *9*, 698876. https://doi.org/10.3389/feart.2021.698876

Liang, X. S. (2014). Unraveling the cause-effect relation between time series. *Physical Review E*, *90*(5), 052150. https://doi.org/10.1103/PhysRevE.90.052150

Liang, X. S. (2015). Normalizing the causality between time series. *Physical Review E*, *92*(2), 022126. https://doi.org/10.1103/PhysRevE.92.022126

Litzow, M. A., Hunsicker, M. E., Bond, N. A., Burke, B. J., Cunningham, C. J., Gosselin, J. L., et al. (2020). The changing physical and ecological meanings of North Pacific Ocean climate indices. *Proceedings of the National Academy of Sciences*, *117*(14), 7665–7671. https://doi.org/10.1073/pnas.1921266117

Liu, Z.-J., Zhu, X.-H., Nakamura, H., Nishina, A., Wang, M., & Zheng, H. (2021). Comprehensive observational features for the Kuroshio transport decreasing trend during a recent global warming hiatus. *Geophysical Research Letters*, *48*(18), e2021GL094169. https://doi.org/10.1029/2021GL094169

Locarnini, R. A., Mishonov, A. V., Baranova, O. K., Reagan, J. R., Boyer, T. P., Seidov, D., et al. (2024). World Ocean Atlas 2023, volume 1: Temperature. *NOAA Atlas NESDIS*, *89*. https://doi.org/10.25923/54BH-1613

Mills, K., Pershing, A., Brown, C., Chen, Y., Chiang, F.-S., Holland, D., et al. (2013). Fisheries management in a changing climate: Lessons from the 2012 ocean heat wave in the Northwest Atlantic. *Oceanography*, *26*(2). https://doi.org/10.5670/oceanog.2013.27

Newman, M., Alexander, M. A., Ault, T. R., Cobb, K. M., Deser, C., Lorenzo, E. D., et al. (2016). The Pacific decadal oscillation, revisited. *Journal of Climate*, *29*(12), 4399–4427. https://doi.org/10.1175/JCLI-D-15-0508.1

Nonaka, M., & Xie, S.-P. (2003). Covariations of sea surface temperature and wind over the Kuroshio and its extension: Evidence for ocean-to-atmosphere feedback. *Journal of Climate*, *16*(9), 1404–1413. https://doi.org/10.1175/1520-0442(2003)16⟨1404:COSSTA⟩2.0.CO;2

Noto, M., & Yasuda, I. (1999). Population decline of the Japanese sardine, Sardinops melanostictus, in relation to sea surface temperature in the Kuroshio extension. *Canadian Journal of Fisheries and Aquatic Sciences*, *56*(6), 973–983. https://doi.org/10.1139/f99-028

Oka, E., Ishii, M., Nakano, T., Suga, T., Kouketsu, S., Miyamoto, M., et al. (2018). Fifty years of the 137°E repeat hydrographic section in the Western North Pacific Ocean. *Journal of Oceanography*, *74*(2), 115–145. https://doi.org/10.1007/s10872-017-0461-x

Oka, E., Katsura, S., Inoue, H., Kojima, A., Kitamoto, M., Nakano, T., & Suga, T. (2017). Long-term change and variation of salinity in the Western North Pacific subtropical gyre revealed by 50-year long observations along 137°E. *Journal of Oceanography*, *73*(4), 479–490. https://doi.org/10.1007/s10872-017-0416-2

Oliver, E. C. J. (2019). Mean warming not variability drives marine heatwave trends. *Climate Dynamics*, *53*(3), 1653–1659. https://doi.org/10.1007/s00382-019-04707-2

Oliver, E. C. J., Benthuysen, J. A., Darmaraki, S., Donat, M. G., Hobday, A. J., Holbrook, N. J., et al. (2021). Marine heatwaves. *Annual Review of Marine Science*, *13*(1), 313–342. https://doi.org/10.1146/annurev-marine-032720-095144

Oliver, E. C. J., Burrows, M. T., Donat, M. G., Sen Gupta, A., Alexander, L. V., Perkins-Kirkpatrick, S. E., et al. (2019). Projected marine heatwaves in the 21st century and the potential for ecological impact. *Frontiers in Marine Science*, *6*, 734. https://doi.org/10.3389/fmars.2019.00734

Oliver, E. C. J., Donat, M. G., Burrows, M. T., Moore, P. J., Smale, D. A., Alexander, L. V., et al. (2018). Longer and more frequent marine heatwaves over the past century. *Nature Communications*, *9*(1), 1324. https://doi.org/10.1038/s41467-018-03732-9

Pathmeswaran, C., Sen Gupta, A., Perkins-Kirkpatrick, S. E., & Hart, M. A. (2022). Exploring potential links between Co-occurring coastal terrestrial and marine heatwaves in Australia. *Frontiers in Climate*, *4*, 792730. https://doi.org/10.3389/fclim.2022.792730

Pershing, A. J., Mills, K. E., Dayton, A. M., Franklin, B. S., & Kennedy, B. T. (2018). Evidence for adaptation from the 2016 Marine heatwave in the Northwest Atlantic Ocean. *Oceanography*, *31*(2), 152–161. https://doi.org/10.5670/oceanog.2018.213

Qiu, B., Chen, S., & Oka, E. (2023). Why did the 2017 Kuroshio large meander event become the longest in the past 70 years? *Geophysical Research Letters*, *50*(10), e2023GL103548. https://doi.org/10.1029/2023GL103548

Qiu, B., Chen, S., Schneider, N., & Taguchi, B. (2014). A coupled decadal prediction of the dynamic state of the Kuroshio extension System. *Journal of Climate*, *27*(4), 1751–1764. https://doi.org/10.1175/JCLI-D-13-00318.1

Reagan, J. R., Boyer, T. P., Garcia, H. E., Locarnini, R. A., Baranova, O. K., Bouchard, C., et al. (2024). World Ocean atlas 2023 [Dataset]. *NOAA National Centers for Environmental Information*. https://doi.org/10.25921/va26-hv25

Ridgway, K. R., Coleman, R. C., Bailey, R. J., & Sutton, P. (2008). Decadal variability of East Australian current transport inferred from repeated high-density XBT transects, a CTD survey and satellite altimetry. *Journal of Geophysical Research*, *113*(C8), C08039. https://doi.org/10.1029/2007JC004664

Roemmich, D. (1983). Optimal estimation of hydrographic station data and derived fields. *Journal of Physical Oceanography*, *13*(8), 1544–1549. https://doi.org/10.1175/1520-0485(1983)013⟨1544:OEOHSD⟩2.0.CO;2

Sasaki, Y. N., Minobe, S., Asai, T., & Inatsu, M. (2012). Influence of the Kuroshio in the East China Sea on the early summer (Baiu) rain. *Journal of Climate*, *25*(19), 6627–6645. https://doi.org/10.1175/JCLI-D-11-00727.1

Scannell, H. A., Pershing, A. J., Alexander, M. A., Thomas, A. C., & Mills, K. E. (2016). Frequency of marine heatwaves in the North Atlantic and North Pacific since 1950. *Geophysical Research Letters*, *43*(5), 2069–2076. https://doi.org/10.1002/2015GL067308

Schaeffer, A., & Roughan, M. (2017). Subsurface intensification of marine heatwaves off southeastern Australia: The role of stratification and local winds. *Geophysical Research Letters*, *44*(10), 5025–5033. https://doi.org/10.1002/2017GL073714

Schaeffer, A., Sen Gupta, A., & Roughan, M. (2023). Seasonal stratification and complex local dynamics control the sub-surface structure of marine heatwaves in Eastern Australian coastal waters. *Communications Earth & Environment*, *4*(1), 1–12. https://doi.org/10.1038/s43247-023-00966-4

Sen Gupta, A., Thomsen, M., Benthuysen, J. A., Hobday, A. J., Oliver, E., Alexander, L. V., et al. (2020). Drivers and impacts of the most extreme marine heatwave events. *Scientific Reports*, *10*(1), 19359. https://doi.org/10.1038/s41598-020-75445-3

Smale, D. A., Wernberg, T., Oliver, E. C. J., Thomsen, M., Harvey, B. P., Straub, S. C., et al. (2019). Marine heatwaves threaten global biodiversity and the provision of ecosystem services. *Nature Climate Change*, *9*(4), 306–312. https://doi.org/10.1038/s41558-019-0412-1

Smith, K. E., Burrows, M. T., Hobday, A. J., King, N. G., Moore, P. J., Sen Gupta, A., et al. (2023). Biological impacts of marine heatwaves. *Annual Review of Marine Science*, *15*(1), 119–145. https://doi.org/10.1146/annurev-marine-032122-121437

Smith, K. E., Burrows, M. T., Hobday, A. J., Sen Gupta, A., Moore, P. J., Thomsen, M., et al. (2021). Socioeconomic impacts of marine heatwaves: Global issues and opportunities. *Science*, *374*(6566), eabj3593. https://doi.org/10.1126/science.abj3593

Sugimoto, S., Qiu, B., & Schneider, N. (2021). Local atmospheric response to the Kuroshio large meander path in summer and its remote influence on the climate of Japan. *Journal of Climate*, *34*(9), 3571–3589. https://doi.org/10.1175/JCLI-D-20-0387.1

Talley, L. D., Pickard, G. L., Emery, W. J., & Swift, J. H. (2011). *Descriptive physical oceanography: An introduction* (6th ed.), Academic Press. https://doi.org/10.1016/C2009-0-24322-4

Tochimoto, E., & Iizuka, S. (2022). Impact of warm sea surface temperature over a Kuroshio large meander on extreme heavy rainfall caused by an extratropical cyclone. *Atmospheric Science Letters*, *e1135*(2), e1135. https://doi.org/10.1002/asl.1135

von Kietzell, A., Schurer, A., & Hegerl, G. C. (2022). Marine heatwaves in global sea surface temperature records since 1850. *Environmental Research Letters*, *17*(8), 084027. https://doi.org/10.1088/1748-9326/ac81db

Von Storch, H., & Zwiers, F. W. (1999). *Statistical analysis in climate research* (1st ed.), Cambridge University Press. https://doi.org/10.1017/CBO9780511612336

Wang, Y.-L., Jin, F.-F., Wu, C.-R., & Qiu, B. (2024). Northwestern Pacific Oceanic circulation shaped by ENSO. *Scientific Reports*, *14*(1), 11684. https://doi.org/10.1038/s41598-024-62361-z

Wang, Y.-L., Wu, C.-R., & Chao, S.-Y. (2016). Warming and weakening trends of the Kuroshio during 1993–2013. *Geophysical Research Letters*, *43*(17), 9200–9207. https://doi.org/10.1002/2016GL069432

Welch, C. B., Malan, N., Mawren, D., Morris, T., Sprintall, J., & Hermes, J. C. (2025). Subsurface manifestation of marine heat waves in the Southwestern Indian Ocean. *Ocean Science*, *21*(4), 1695–1708. https://doi.org/10.5194/os-21-1695-2025

White, W. B., & Tai, C.-K. (1995). Inferring interannual changes in global upper ocean heat storage from TOPEX altimetry. *Journal of Geophysical Research*, *100*(C12), 24943–24954. https://doi.org/10.1029/95JC02332

Willis, J. K., Roemmich, D., & Cornuelle, B. (2003). Combining altimetric height with broadscale profile data to estimate steric height, heat storage, subsurface temperature, and sea-surface temperature variability. *Journal of Geophysical Research*, *108*(C9). https://doi.org/10.1029/2002JC001755

Xu, Q., Liu, K., Wang, H., & Chen, X. (2024). Vertical structures and drivers of marine heatwaves and cold-spells in the Kuroshio extension region. *Environmental Research Letters*, *19*(5), 054015. https://doi.org/10.1088/1748-9326/ad3b26

Yatsu, A. (2019). Review of population dynamics and management of small pelagic fishes around the Japanese Archipelago. *Fisheries Science*, *85*(4), 611–639. https://doi.org/10.1007/s12562-019-01305-3

Yoshida, T., Shimohira, Y., Rinno, H., Yokouchi, K., & Akiyama, H. (2006). Criteria for the determination of a large meander of the Kuroshio based on its path information. *Oceanography in Japan*, *15*(6), 499–507. https://doi.org/10.5928/kaiyou.15.6_499

Zhang, Y., Du, Y., Feng, M., & Hobday, A. J. (2023). Vertical structures of marine heatwaves. *Nature Communications*, *14*(1), 6483. https://doi.org/10.1038/s41467-023-42219-0

Zhou, C., Ren, H.-L., Geng, Y., Wang, R., & Wang, L. (2024). Seasonal predictability of SST anomalies and marine heatwaves over the Kuroshio extension region in the Copernicus C3S models. *Ocean Modelling*, *189*, 102361. https://doi.org/10.1016/j.ocemod.2024.102361

Zilberman, N. V., Scanderbeg, M., Gray, A. R., & Oke, P. R. (2023). Scripps Argo trajectory-based velocity product: Global estimates of absolute velocity derived from core, biogeochemical, and deep Argo float trajectories at parking depth. *Journal of Atmospheric and Oceanic Technology*, *40*(3), 361–374. https://doi.org/10.1175/JTECH-D-22-0065.1